Int J Adv Manuf Technol (2016) 83:1637–1647
DOI 10.1007/s00170-015-7695-9

ORIGINAL ARTICLE

Formation characteristic, microstructure, and mechanical performances of aluminum-based components by friction stir additive manufacturing

Mao Yuqing[1] · **Ke Liming**[1,2] · **Huang Chunping**[2] · **Liu Fencheng**[2] · **Liu Qiang**[1]

Received: 19 May 2015 / Accepted: 3 August 2015 / Published online: 18 August 2015

Abstract In this study, a new solid-state technique of friction stir additive manufacturing (FSAM) based on friction stir welding (FSW) principle was used to build successfully a multilayered stack of an Al-based component. The results show that a hook stretches into the nugget zone on advancing side, while it moves upwards to the periphery on retreating side for a single-level welding. With manufacturing the second layer, the hooks bend outward significantly attributing to the extrusion of above plastic material, which can avoid the hook to stretch into the stirred zone. A transition zone (TZ) is also formed near the interface between two layers. In addition, fine equiaxed grains are observed due to the dynamic recrystallization in the whole. However, a difference in grain size still exists through the build direction and in the TZ is forming coarse band grains. A similar change occurs in the precipitate morphology, size, and distribution. Form the top to the bottom, the microhardness changes dramatically, and a maximum 115 HV at the top is obtained. The tensile strength of all the slices increases and the elongation decreases slightly in comparison of Al substrate, and the slice top has the highest mechanical properties, which is attributed to fine grains and desirable precipitate characterization.

✉ Ke Liming
liming_ke@126.com

Mao Yuqing
maoyuqing1987@mail.nwpu.edu.cn

[1] State Key Laboratory of Solidification Processing, Northwestern Polytechnical University, Xi'an 710072, People's Republic of China

[2] National Defence Key Discipline Laboratory of Light Alloy Processing Science and Technology, Nanchang Hangkong University, Nanchang 330063, People's Republic of China

Keywords Friction stir additive manufacturing · Aluminum substrate · Formation characteristic · Microstructure · Mechanical properties · Fracture morphologies

1 Introduction

A total of 7075 aluminum alloy, as a precipitation hardened, wrought material based on Al-Mg-Zn-Cu system, which is considered as one of the strongest aluminum alloys. Meanwhile, due to the attractive combination of excellent weldability, high strength to weight ratio, high heat conductivity, and good corrosion resistance, AA7075 has been widely used to produce some components in aviation, aerospace fields, and domestic industries [1, 2]. However, a few aluminum matrix parts pertaining to the cabin and cockpit are normally in irregular and complex configurations, which are difficult to fabricate by the conventional processing methods such as casting processes. In addition, during the conventional casting processes, coarser and heterogeneous microstructures and large degrees of segregation are very easy to generate due to the slow solidification rates [3, 4]. Therefore, such applications of the traditional casting processes are limited, and some new processing methods are highly desired to cater to the need for obtaining complex components with fine and uniform microstructures and the stringent performance requirements laid by the aviation industry.

Additive manufacturing (AM), defined as the process of joining materials to make objects from three-dimensional (3D) model data, is a new generation of manufacturing processes in which some parts are fabricated by layer-by-layer addition of materials as opposed to traditional subtractive manufacturing methodologies, such as machining or material deformation processes, and is considered to be the most significant manufacturing approach to have emerged in the last

few decades [5–7]. The AM technology attains considerable recognition and adoption in various industry sectors ever since the first AM process is introduced in late 1980s [8]. Such a spur in the field of additive manufacturing is realized by the combination of several techniques and comprehensively documented in some review papers [9–11]. Though additive manufacturing comes to the forefront by virtue of several innovations that paves its way, lots of key challenges still persist. For the metal-based additive technologies, some special attentions are laid on the specific characteristics such as build rate, build volume, layer thickness, and the overlapped structure between layer and layer.

At present, several metal-based additive technologies include mainly shaped metal deposition [12], laser additive manufacturing techniques [13], and electron beam melting [14], which are heavily used to fabricate majority of multilayered metal parts. On the one hand, shaped metal deposition can lead to higher production rates, but it is at the expense of surface finish and dimensional accuracy. Moreover, when laser additive manufacturing techniques is applied, though a good surface finish is obtained, the process is still limited due to higher operating costs, low production rate, and small build volumes. On the other hand, some components produced by electron beam deposition perform better mechanical properties, but it is limited to use owing to the cost factor pertaining to the use of inert atmosphere. Other issues include that powder particles-based substrate used in all the three techniques are usually contaminated; during the additive process, the substrate is melt into the liquid, and it is easy to form internal porosity, inclusions, and other solidification defects. In addition, the microstructures of the manufactured component are extremely inhomogeneous and its structural properties are spatially dependent [15, 16]. Other techniques such as ultrasonic additive manufacturing have the ability to produce multi-material components, but the microstructures are highly nonuniform and there exist great differences between the interfaces and interfaces or noninterfaces, so the mechanical properties are inferior compared with base material [10]. Therefore, a desired requirement for any manufactured component is necessary to possess a homogeneous microstructure and better properties.

Friction stir additive manufacturing (FSAM), as a new environmentally friendly, energy-effective solid-state process technology based on friction stir welding (FSW), has a huge potential to fabricate lightweight materials with high structural performances [17]. In FSAM process, the metal substrates such as aluminum/magnesium alloys are being processed but do not melt and recast, which can avoid efficiently some internal porosities and solidification defects. The fundamentals of FSAM procedure are easily understood, and it is similar to the FSW process while it differs in their respective functions. In general, a nonconsumable rotating tool with a special pin and shoulder is inserted into slowly the overlapping surfaces of the plates/sheets and subsequently moves forward along the joint line to be joined. The schematic of the FSAM process is shown in Fig. 1. Furthermore, the necessary heat to weld aluminum substrates is provided by the frictional heat between the rotating shoulder and the workpiece and the deformation heat achieved by the motion of the pin, which makes metal substrate deform to result in a circulatory flow of plasticized materials around the pin surface. The plasticized materials underneath the shoulder are subjected to extruding by the rotation and the traverse movement of the pin from the advancing side to the retreating side, and the weld nugget is formed, while its macro shape is depended on the geometrical features of the pin. Currently, the reports relating to FSAM technology are extremely limited. The friction joining used for the additive manufacturing is under the patent, but it is only an assumption as a possible route to build 3-D layers [18]. Palanivel et al. [19] reported recently that the FSAM as a potential technique can attain efficiently Mg-based components with high structural performances through controlling the microstructures. But, the reports of friction stir additive manufacturing Al-based parts are not pursued leading to a lack of literatures about FSAM, and some further studies such as the formation quality, defects, and microstructure evolution are also lacked. Therefore, the aim of this study is to investigate a multilayered build of an Al substrate obtained by FSAM technique, and sequentially, stacking layers are performed over the previously processed layer. For the purpose, a sound tool is designed to join the Al plates, and the formation characterization, microstructure evolution in the interfaces, and noninterfacial zones and mechanical properties of the FSAM Al-based component are further studied.

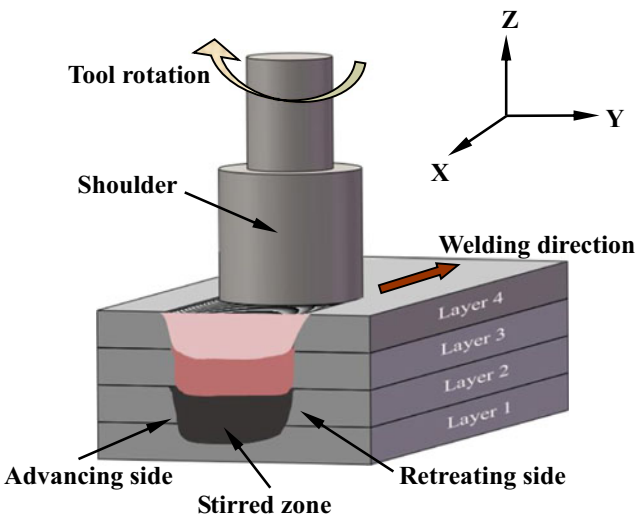

Fig. 1 Schematic illustration of friction stir additive manufacturing (FSAM) process

2 Experimental procedures

In the present study, 5-mm thick plates of 7075 aluminum alloy in annealed condition were used as base material to additively manufacture. The nominal chemical compositions of AA7075-O are listed in Table 1, and the tensile strength and elongation of AA7075-O plate are 225 MPa, 17.9 %, respectively. The plates with a size of 200×40×5 mm were prepared for longitudinally friction stir lap welding on a modified horizontal-type milling machine, and the welding direction was parallel to the rolling direction. A stack of nine layers with a height of about 42 mm was produced by sequentially building and machining of the lap welded layers. FSAM was carried out using a tool made of GH4169 steel with a concave-shaped shoulder and a left cylindrical threaded pin made. The shoulder diameter was 30 mm, and the pin diameter and pin height were 14 and 5.2 mm, respectively. Meanwhile, a constant tilt angle of the rotating tool of 2° from the vertical axis of FSW machine was used to contain the material beneath the shoulder, and a plunge depth of 0.2 mm of the pin was kept. The same welding parameters such as a constant rotation speed of 600 rpm and a fixed traverse speed of 60 mm/min were used during FSAM (the process parameters were optimized after lots of trial and error).

The specimens for metallographic examination and hardness evaluation were cross-sectioned from the welded layers perpendicular to the welding direction, which were ground and polished following a standard metallographic process. The microstructural features in different positions were observed by etching in a mixed acid solution of 5 ml nitric acid, 3 ml hydrochloric acid, 2 ml hydrofluoric acid, and 190 ml water for duration of 20 s. Microstructural characterization and secondary phase particles analysis were extensively performed by employing a TESCAN VEGA II-LMH scanning electron microscope (SEM) equipped with an energy dispersive X-ray spectroscopy (EDX) system and a JEOL 2010 transmission electron microscope (TEM) operating at 200 keV. For TEM analysis, the samples of 3-mm circular disks were prepared by twin-jet electro-polish in a solution of 25 vol% of HNO_3 and 75 vol% of methanol at −30 °C, and the voltage of 12 V was set up. The hardness along different build direction from the bottom to top of the cut sample was measured using a HX-1000 model hardness tester at a load of 0.98 N with a 10-s dwell time, and these measurements were performed along the centerline in the cut build direction at an interval of 0.5 mm (*Z* axis). As per the ASTM, B557M-10, tensile test samples were cut parallel to three directions (*X*, *Y*, and *Z* axis) using the wire-cutting electrical discharge machine, and subsequently machined to prepare tensile specimens. This was done to estimate the strength and ductility of different parts of the FSAM component in comparison of Al substrate. The gage dimension for the tensile sample was 40×10×6 mm, as shown in Fig. 2. The tensile tests were performed at room temperature using a WDS-100 testing machine at an initial strain rate of 1 mm/min, and the average value of three specimens was reported. The fracture surfaces of the tensile samples were analyzed by SEM technique.

Table 1 Chemical composition (wt%) of AA7075-O substrate

Mg	Zn	Cu	Si	Fe	Mn	Cr	Ti	Al
2.7	5.65	1.7	0.4	0.5	0.3	0.22	0.2	Balance

3 Results and discussion

3.1 Formation characteristic

Figure 3 shows the macrostructures of the cross sections of different FSAM components and particular sections of high-resolution images. Among them, a macrograph of the friction stir lap welded joint is shown in Fig. 3a. Also, the cross section of the FSAM component involving nine layers stack is shown in Fig. 3b, and the local magnified figures of different parts in the component are shown in Fig. 3c–f, respectively. From the images, it is seen clearly that some obvious defects such as hook and kiss bonding are observed for a single friction stir lap welded joint. Similar results were also reported by Salari et al. [20]. Since FSAM is considered to be a multiple friction stir lap welding process, the complex feature of the material flow results in various kinds of defects. For the single friction stir lap weld, one of the most common defects observed in the interfaces between two welded plates is hook, and it moves towards to thermo-mechanically affected zone (TMAZ) or weld nugget zone (WNZ). In fact, hook is a kind of inherent feature and which is characterized as a crack-like unbonded interface that deformed from the original faying surfaces on the advancing side (AS) and retreating side (RS), as shown in Fig. 3a. Meanwhile, there is a visible difference in the movement direction of the hook, on the AS the hook stretches into the WNZ, while it moves upward to the TMAZ on the RS. However, for the multiple lap joints, it is obviously seen from Fig. 3b–f that the hook on two sides moves upwards and does not stretch into the center stirred zone. From the local magnifications, some overlapped transition zones under each interface and a kiss bonding adjacent to the top periphery are found in Fig. 3d, e. The main reason is resulting from the complicated material flow during FSAM.

In the present study, the formation of the hook in a single lapped joint is related to the material flow in the stir zone affected by the pin with left hand thread and can be interpreted as the following discussions. On one hand, the stir zone is formed attributing to the cooperation of three material movement processes: Firstly, the stirred material of the lower plates moves upwards and subsequently incorporate with the

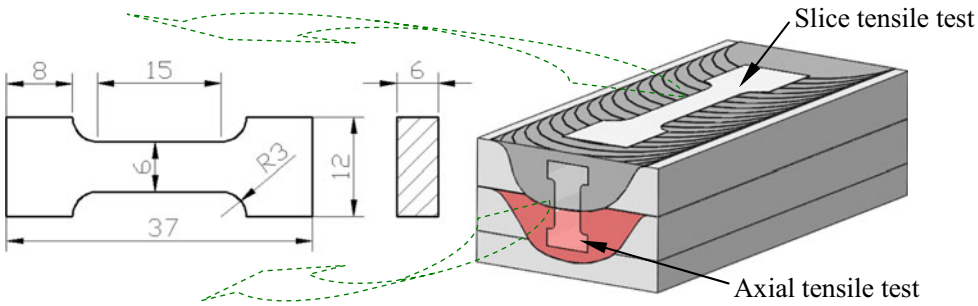

Fig. 2 Dimension of the tensile specimen

material of the upper plate, secondly, the incorporated materials move downwards spirally along the left thread pin, and finally, the incorporated materials of the upper and lower plate release from the bottom of the pin, and the above steps are repeated. On the other hand, the faying surfaces of both plates are vertical to the tool, which makes the oxide layers at the interfaces more difficult to be crumbed sufficiently than those in butt welding. As more materials move upwards from the lower plates and incorporate with the upper plate material, the stirred zone becomes larger and larger. The original interfaces on both sides are extruded upwards into the stir zone, which is associated with changes in material flow direction, from downward to upward, depending on the tool geometry and welding condition [21]. Consequently, a hook-shaped macrostructure is formed, and the schematic diagram of the hook formation is shown in Fig. 4a. During FSAM, when another plate is additively manufactured, other incorporated materials move downward along the pin and extrude the hook expanding into the stir zone. In turn, the hook is bent upward into the TMAZ due to the upward flow of the material induced by the tool pin, and the driving force of the upward lower plates is provided by the shoulder penetration into the surface of the upper plate and the pin penetration into the lower plate during the dwell period, and the schematic diagram of hook deformation is shown in Fig. 4b. Similar results were reported by Badarinarayan et al. [22] and Yin et al. [23]. Furthermore, the formation of the kiss bonding is owing to the insufficient flow resulted from the incomplete stirring of the pin. While the generation of the overlapped transition zone beneath the pin is associated with welding thermal cycle due to a secondary stirring of the pin, a simple schematic is also shown in Fig. 4b.

3.2 Microstructure evolution in different regions

For the FSAM components, the feature of the material flow is very complex due to involving multiple layers lap joints which are suffering from varying degrees of thermal cycles. As a consequence, some differences in the microstructures in different noninterfaces and interfaces between layer and layer still exist. In order to observe the microstructure evolution in the different positions, the FSAM component is conventionally cross-sectioned, and then a center stirred zone with a size of 10×35×2 mm is cut off, as shown in Fig. 5b. From the picture, it is clearly seen that there is no defects in the center stirred zone. Whereafter, the microstructures of the cut structure corresponding to the different positions in Fig. 5b are observed by optical microscope, as shown in Fig. 6. For the FSAM process, the original microstructure of Al substrate plays an important role in the subsequent microstructural evolution, which is characterized by coarser banded grains arranged along the rolling direction in Fig. 6a. However, experiencing high peak temperature, strain rate, and the welding thermal cycle, FSAM leads to dissolution, coarsening, and dynamic recrystallization, and these processes could

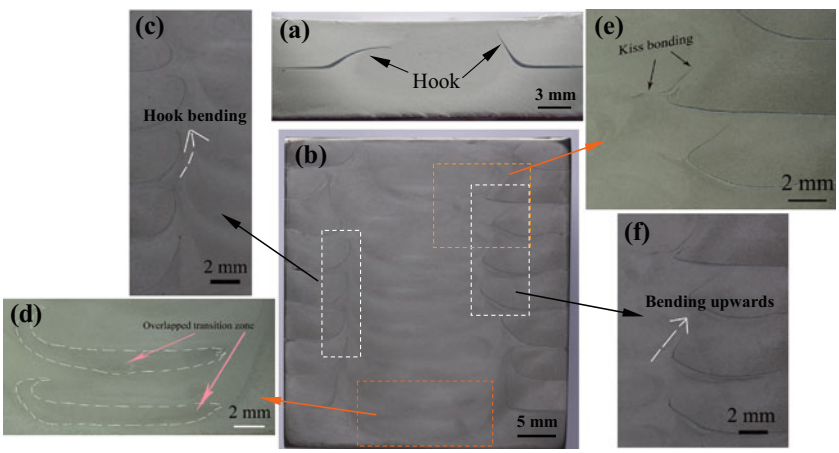

Fig. 3 Formation morphologies on the cross section: **a** a single lapped joint, **b** a FSAM component with nine layers stack, and **c**–**f** local magnifications in **b**

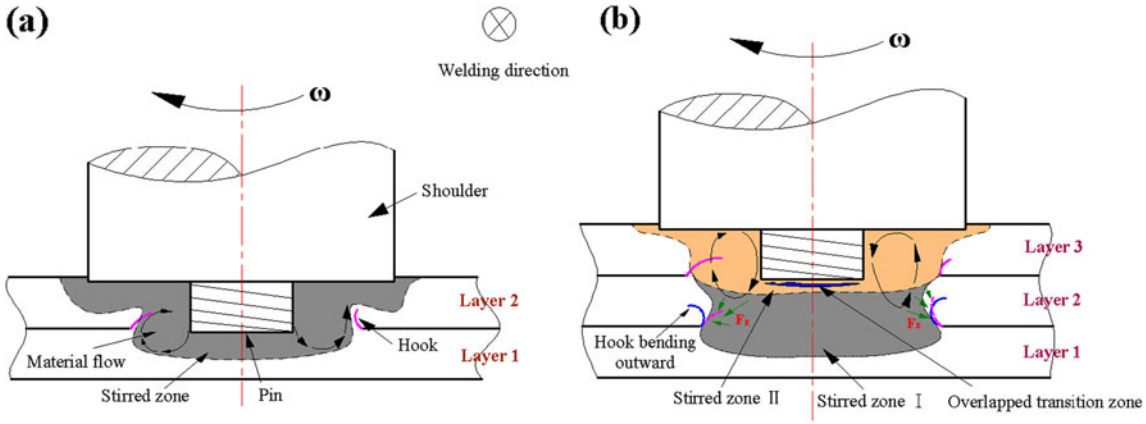

Fig. 4 Schematic diagram of metal flow: **a** hook formation and **b** hook bending and deformation

occur simultaneously. Seen from the micrographs, it is found that after FSAM, the stirred zone is characterized by a typical feature with fine equiaxed grains owing to dynamic recrystallization. Moreover, the microstructure evolution is a very complex process described as follows: (1) At the initial stage, the parent grains split into coarse band structures. As the strain increases, some new elongated fibrous grains are formed, and then a finer scale is produced when further grain subdivision occurs continuously; (2) with increasing the temperature to the tool, fine nugget scale grains are formed from closely spaced parallel HAGBs. The bands of fine grains are forced together and increase in volume fraction with strain; (3) finally, the unstable fibrous grain fragments form a full nugget-like microstructure consisting of low aspect ratio ultrafine grains. Following welding, the grains become more equiaxed and are coarsened slightly due to static annealing [24, 25], whereas some subtle differences in the microstructures between the noninterfaces and interfaces along the build direction are found from Fig. 6b–h corresponding to the locations annotated in Fig. 5b, respectively. Obviously, the grain size in different positions is significantly different. From Fig. 6b, the size in the shoulder zone is somewhat bigger than that of the center zone for a single welding joint. The main reason is that fine recrystallized grains in the shoulder zone are coarsened due to bigger forging forces, higher peak temperature, and longer cooling times. In addition, as seen from Fig. 6c, d, the grain size is also various, and the grains in the ninth noninterface are smaller than that in the interface. There exists a new transition zone where a banded structure is formed with lots of coarser grains. Preliminary analysis suggests that the interface undergoes the second stirring action of the pin when another plate is additively manufacturing and coarse grains in the original shoulder zone are refined to a degree, while the size in the interface is still larger than that in the noninterface due to longer time of thermal cycle. The formation of the transition zone adjacent to the interface is attributed to plastic flow of warmer materials and multiple thermal cycles during FSAM. Furthermore, it is obvious that the grain size increases from the top to the bottom through the thickness direction. The explanation is that, when other plates are additively manufacturing layer by layer, those regions at the bottom have to suffer from more thermal cycle and longer time of static annealing, which result in more serious coarsening of fine recrystallized grains and precipitated particles.

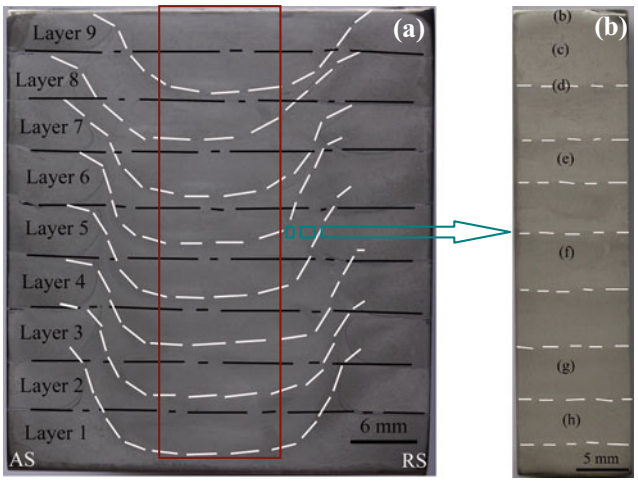

Fig. 5 Macro-figures of the cross sections: **a** a complete FSAM component and **b** a cut part for microstructural observation

3.3 Secondary phase distribution

To examine the differences in secondary phase distribution of each local position in the FSAM component, SEM analysis is done and the micrographs are shown in Fig. 7b–h, respectively. Compared to that of Al substrate in Fig. 7a, the particles in different positions are more uniform and dispersive. As the material after FSAM experiences severe plastic deformation and high temperature, the coarse strengthening particles are subjected to breaking up, dissolving and precipitating. In most cases, these processes occur concurrently. Therefore, fine precipitated particles are dispersively distributed in the stirred zone, as shown in Fig. 7. By EDX microanalysis, these precipitate phases (white particles) comprise of possible η

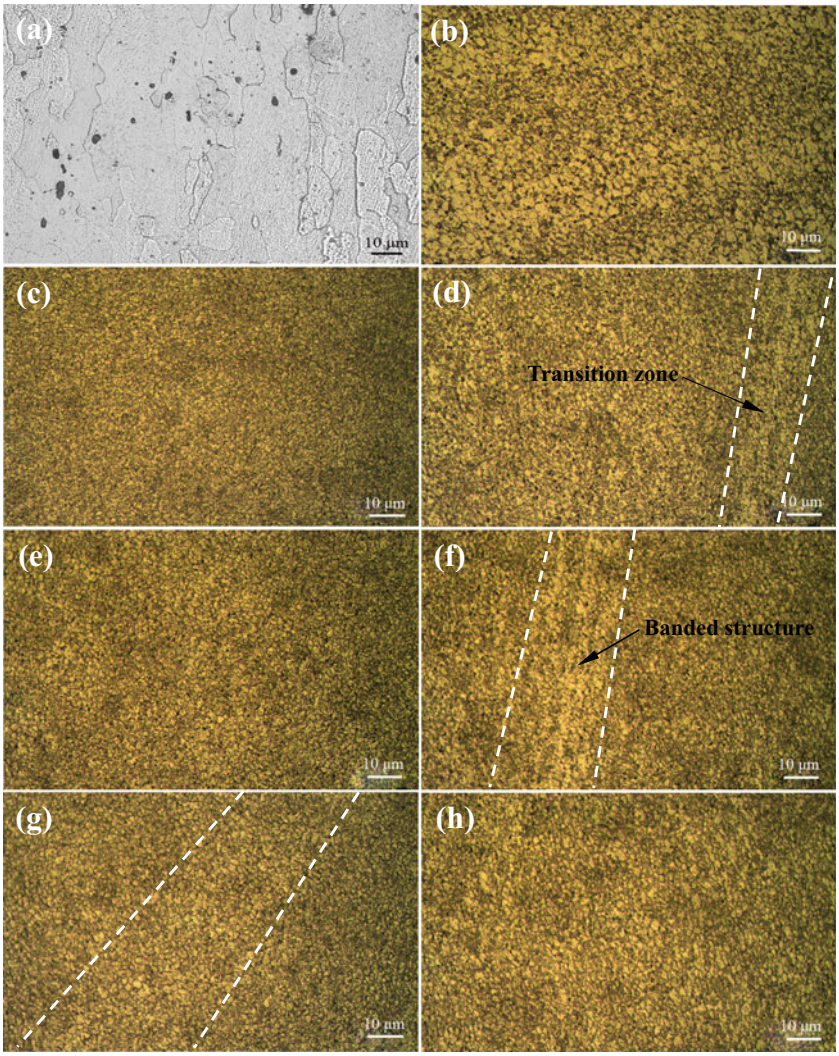

Fig. 6 Microstructure in different positions: **a** Al substrate, **b** the top in the part, **c** in layer 9, **d** in interface 9, **e** in layer 7, **f** in layer 5 close the transition zone, **g** in layer 3 adjacent to transition zone, and **h** in layer 2

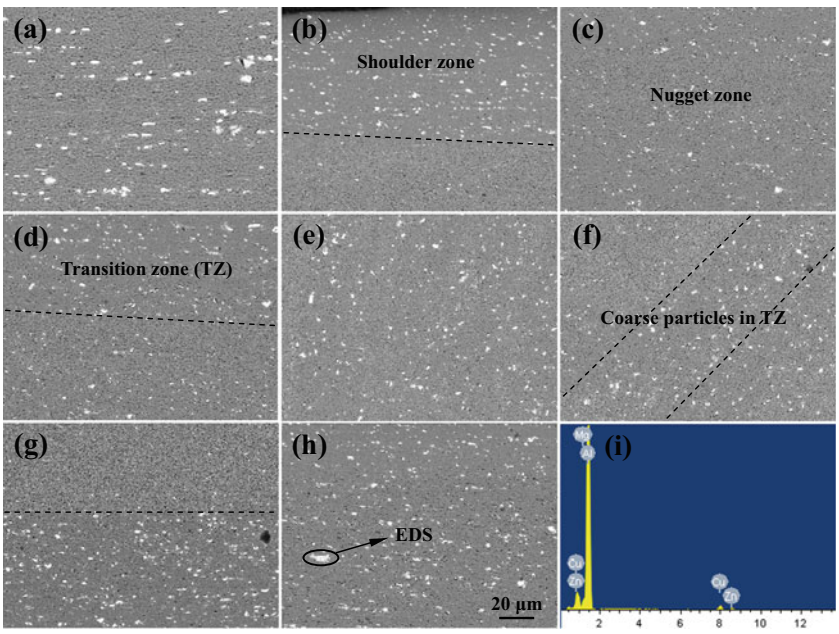

Fig. 7 BSE images of precipitate distribution in different zones: **a** Al substrate, **b** the top in the cut part, **c** in layer 9, **d** in interface 9, **e** in layer 7, **f** in layer 5 close the transition zone, **g** in layer 3 adjacent to transition zone, **h** in layer 2, and **i** EDS in **h**

($MgZn_2$) and T (AlZnMgCu) phases in Fig. 7i. Meanwhile, Fig. 7b–h shows a considerable difference in particles size in the noninterfaces and interfaces. The precipitated particles in the shoulder zone are bigger than that in the center stirred zone, as shown in Fig. 7b, c, e, h. On one hand, Fig. 7c, e, h refers to the pin dominated flow regimes and are representative of a single pass welding. Where the metals experience high temperature and great stirring force, such high strain rate coupled with high temperature may lead to sufficient dissolution of original secondary phase particles in the Al substrate. Also, the peak temperature above the solvus coupled with a high cooling rate aids grain boundary diffusion at a lower temperature leading to precipitation at grain boundaries. However, on the other hand, the shoulder zone dominated plastic flow at the upper is subjected to more frictional heat supplied by virtue of the shoulder geometry and longer cooling times, which can lead fine precipitates to coarsening and growing up abnormally during subsequent static annealing. In addition, the banded precipitate particles are observed adjacent to the interfaces from Fig. 7d, f, g. This may imply that the strain rate and cooling rate experienced by the interfaces must be lower in comparison to the individual layers.

To analyze further, TEM analysis is done to evaluate precipitate morphology, size, and dislocation densities, and confirm which type these precipitated phases are in different zones. Figure 11 shows TEM micrographs of different specimens of the FSAM component divided into three parts marking as the upper, middle, and lower, respectively. Seen from the images, some smaller precipitated phase particles and a higher dislocation density are found at the upper, as shown in Fig. 8a, d, respectively. However, at the lower, refined precipitates are coarsened seriously and got to cluster due to undergoing more thermal cycles. By the electron diffraction pattern, we can distinguish that the elliptic particle is a typical η phase in 7xxx series aluminum alloys, which is consistent with the results reported in [24, 26]. The supersaturated solid solution is decomposed mainly in the following sequence: supersaturated solid-solution→GP zone→η' ($MgZn_2$)→η ($MgZn_2$). Moreover, the fact of a higher dislocation density is in agreement with a large amount of strain that the material experiences at the upper. Nonetheless, a great decreasing in dislocation density proves that more recrystallizations occur in the lower part due to more static annealing, which is reflected from the microscopic images in Fig. 6.

3.4 Microhardness profiles

For FSAM component based on 7075-O aluminum alloy, the microstructure change is characterized by the hardness variation, and the mechanical performances are also compared. Figure 9 shows the microhardness profiles of the component after FSAM, and the curves in Fig. 9a represent the hardness distribution along the horizontal direction in different build thickness; however, Fig. 9b reflects the hardness change along build thickness direction in the center zone. The hardness of Al substrate is in the range of 58–65 HV. It is interesting that there is a significant increasing trend in the hardness from the bottom to the top of the FSAM component. The maximum hardness of 102 HV is obtained on the top; nevertheless, the minimum value is found in the bottom close to the base material. The top is obviously harder than the bottom, as shown in Fig 9a. Meanwhile, a similar variation trend in the hardness is presented in Fig. 9b, but the hardness in each overlapped transition zone decreases slightly.

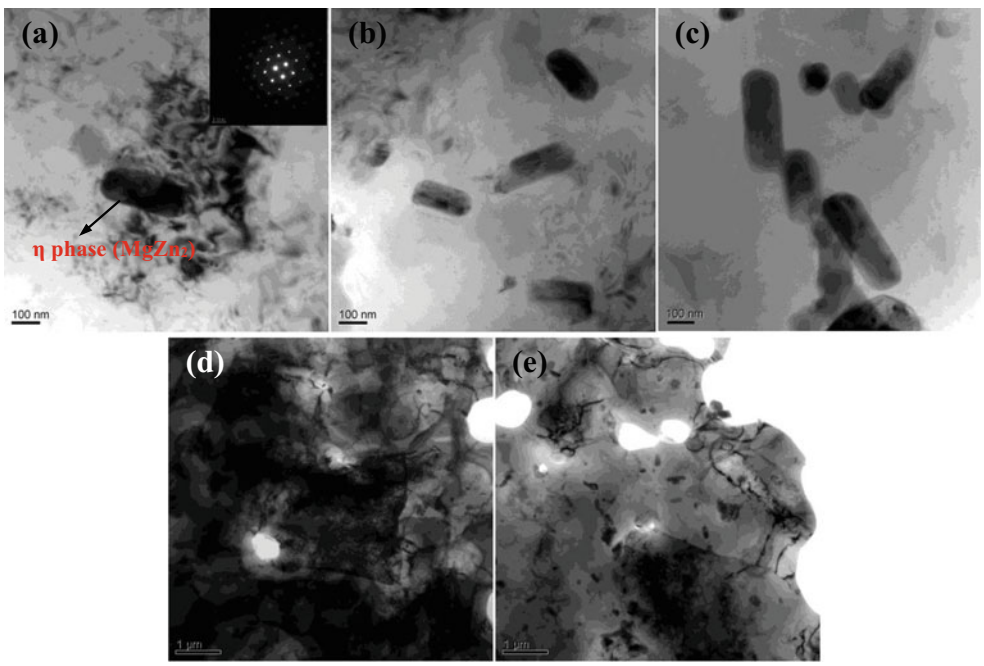

Fig. 8 TEM images showing precipitate size, shape, and distribution in **a** the upper, **b** the middle, and **c** the lower and dislocation densities of **d** the upper and **e** the lower part of the FSAM component

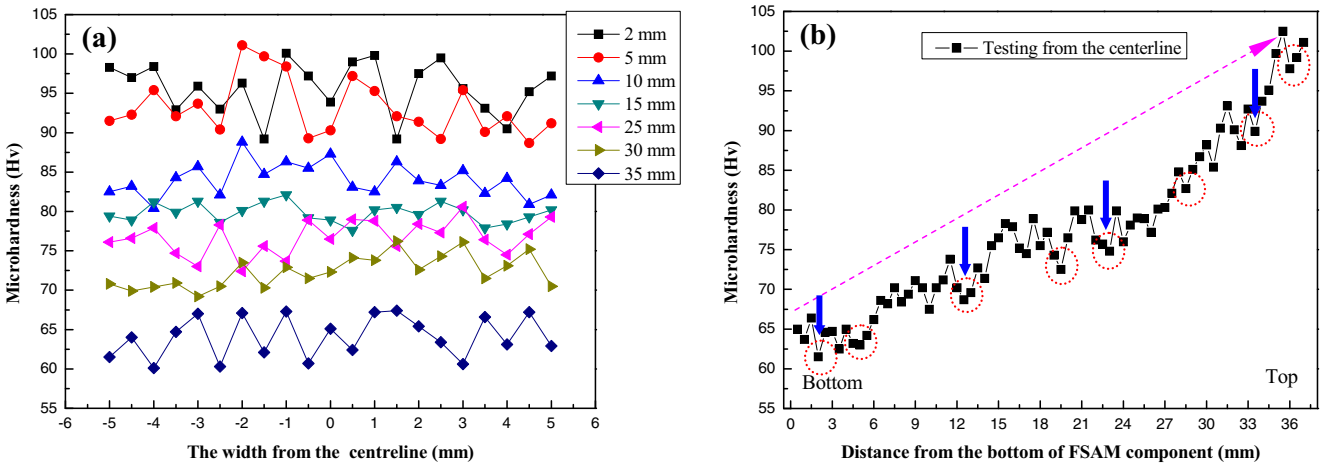

Fig. 9 Microhardness profiles of the cut part: **a** at the horizontal direction and **b** along the build direction

Generally speaking, for the precipitation-strengthened 7075-O aluminum alloy, FSW cannot cause softening in the stirred zone as observing for solid-solution hardened aluminum alloys.

Whereas experiencing high temperature and severe plastic deformation, fine equiaxed grains are generated in the stirred zones. As a consequence, the hardness of the stirred zones is all higher than the Al substrate according to the Hall-Petch relationship ($H_V=H_0+\kappa_H d^{-1/2}$, where H_V is the hardness, d is the grain size, and H_0 and κ_H are the contents) [27]. Moreover, after FSAM, the precipitated particles are smaller and more homogeneous, which helps to improve the hardness. Seen from Fig. 9, the hardness of the whole component presents an asymmetrical distribution along the thickness direction, and there is an obvious decreasing from the top to the bottom. This fact is because, with further manufacturing Al plates continuously, the stirred zone in the bottom undergoes multiple thermal cycles which is similar to a continuous static annealing. The fine recrystallized grains and precipitated particles in these regions are coarsened to different degrees, which are seen clearly from Figs. 6 to 7. Also, the same phenomenon occurs in those overlapped transition zones adjacent the interfaces. Due to suffering from the second stirring of the pin, the grains and particles coarsening can result in a slight decreasing in the hardness of each transition zone (blue arrows in Fig. 9b).

3.5 Mechanical performances

For the FSAM process, the aim is to obtain a complete and defect-free Al-based component with better mechanical performances, so the properties changes of different regions are evaluated. Figure 10 shows the change curves of different slices and axial tensile samples. Furthermore, the engineering stress-strain curves of the tensile specimens are represented in Fig. 10a, and the results including the strength and elongation of the tensile tests are compared in Fig. 10b, which are the average values based on three tests. It is clearly shown that the ultimate tensile strength (σ_b) of FSAM parts increases observably compared to base material, but the elongation (δ) decreases slightly. The maximum σ_b of the slice locates at the top, which reaches to 278 MPa, while the minimum σ_b of 231 MPa presents in the bottom. However, the results of the ductility are opposite, which are 10.4 and 14.8 %, respectively.

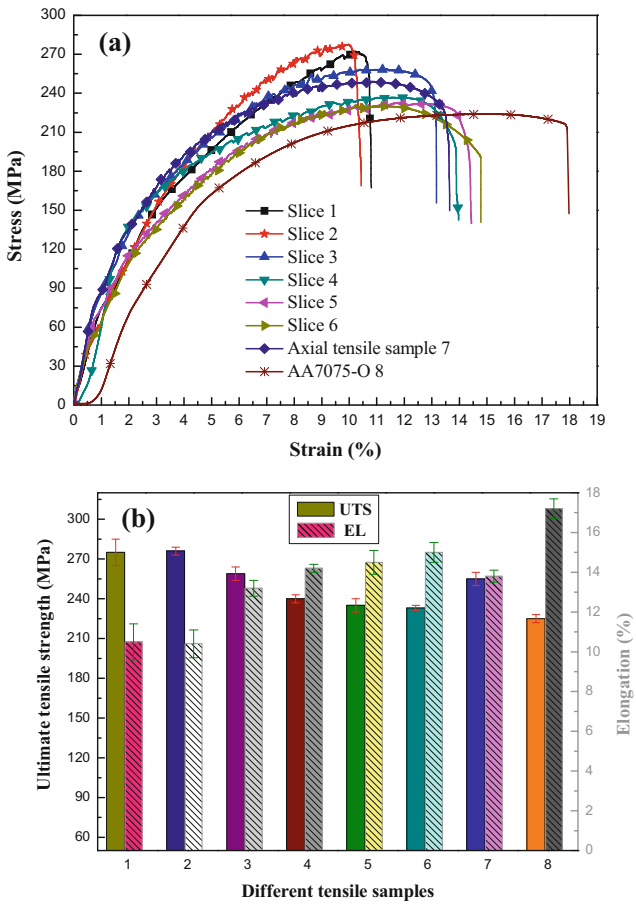

Fig. 10 Mechanical performances of the FSAM component: **a** stress-strain curves and **b** ultimate tensile strength and elongation

As the Al substrate experiences intensive plastic deformation and high temperature during the FSAM process, fine equiaxed grains and uniform precipitated particles are formed in the stirred zones (in Figs. 6 and 7). In the meantime, during FSAM, severe plastic deformation can increase the internal dislocation concentration, and high temperature enhances the interactions between the dislocations and other crystalline imperfections, which may increase the resistance force to the dislocation motion [24, 28]. Therefore, during the tensile test process, fine grains can increase the distance of dislocation migration and decrease the generation of dislocation pile-ups. And, more uniform and dispersive precipitated particles hinder the dislocation motion, which decreases the stress concentration and hardly creates the microcracks at the grain boundaries. Even if the microcracks produce, a higher resistance to propagation can improve the strength of the FSAM component. The decreasing of the slices at the bottom is because that the grains and precipitated particles are coarsened significantly due to continuous static annealing, which is possible to generate lots of the stress concentration and microcracks [29].

3.6 Fracture morphologies

The fracture surfaces of the tensile specimens including different slices and Al substrate are characterized by using SEM, and the fracture morphologies are shown in Fig. 11. It is obvious that the fracture surface of Al substrate consists of

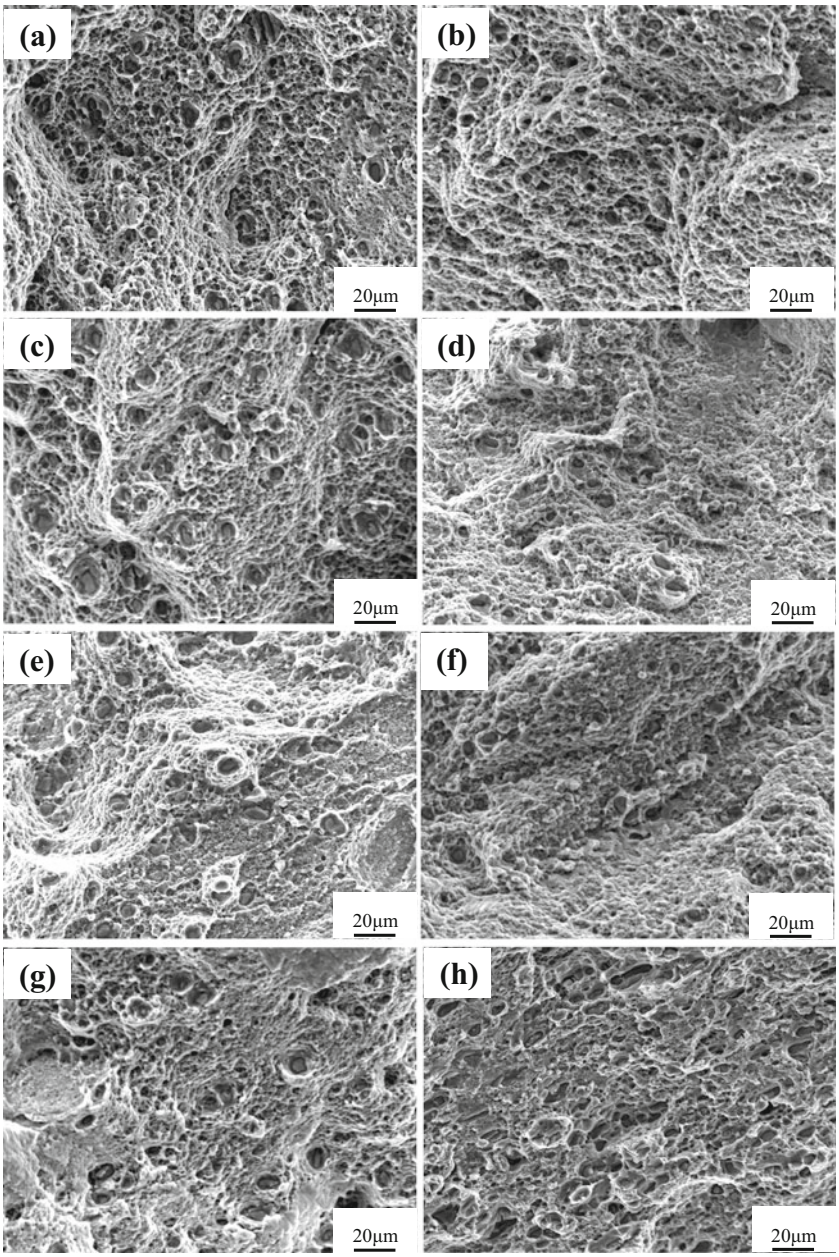

Fig. 11 SEM micrographs of the slices: **a** slice 1 sample, **b** slice 2 sample, **c** slice 3 sample, **d** slice 4 sample, **e** slice 5 sample, **f** slice 6 sample, **g** axial tensile sample, and **h** AA7075-O tensile sample

dimples having various sizes and shapes, and an array of coarser secondary phase particles with elongated shape are peeling off, as shown in Fig. 11h. Moreover, the dimples in the top slices are deeper, and tearing edges are thicker with lots of micropores, which is an indication that the failure is ductile shown in Fig. 11a, b. However, compared with the top and middle slices, fewer dimples and fewer tearing ridges are presented in the fracture surfaces of the bottom slices, and few voids of different sizes and shapes are found in Fig. 11e, f. These facts indicate that the failures have a brittle fracture pattern of quasi-cleavage with river patterns. The main reason is that the presence of coarser precipitates at the grain boundaries is prone to initiate cracks under lower stress during the tensile deformation. For the ductile tensile specimen, it is possible to sustain the tensile load attributing to thicker tear ridges, while the brittle sample fails immediately after a commencement of void coalescence.

4 Conclusions

A new method of friction stir additive manufacturing (FSAM) was used successfully to fabricate a multilayered stack aluminum alloy component with a higher strength. The formation feature, microstructure, and mechanical performances of the FSAM component were investigated. Based on the results obtained by experimental results and theoretical analysis, the following conclusions can be drawn:

1. For a single pass joint, a hook stretches into the nugget zone on advancing side, while it moves upwards on retreating side. With manufacturing another plate continuously, the hooks bend outward owing to the extrusion of new plasticized material coming from upper plate, which can avoid the hook to insert into the center of friction stirred zone. Therefore, an almost complete Al-based component of nine layers stack is fabricated.
2. The dynamic recrystallization leads to fine and equiaxed grains in the stirred zone. However, a difference in grain size occurs in different positions, and the grains at the top are finer, while the bottom grains are coarsened due to static annealing. Moreover, some coarser banded grains are produced in overlapped transition zones. The precipitated particles present a similar trend in morphology, size, and distribution.
3. Compared to Al substrate, the tensile strength of FSAM parts increases significantly, while the elongation decreases slightly. Along the build direction, the strength of the slice increases gradually, and a maximum 279 MPa is obtained at the top. The whole Al-based component performs a higher strength than Al substrate, which is corresponding to the hardness profiles.
4. The fractographs show that plenty of dimples of various sizes, shapes, and thicker tearing ridges present in the top specimen, but the bottom slice present a brittle fracture pattern of quasi-cleavage with river patterns. The failures of the slice specimens show a mixed brittle-ductile fracture mechanism.

Acknowledgments This work was supported by the National Natural Science Foundation of China (NSFC) (No. 51265043, 51265042, and 51364037), the Landed Plan of Science and Technology in Colleges and Universities of Jiangxi Province (No. KJLD12074 and 13055), the open found of the National Defence Key Discipline Laboratory of Light Alloy Processing Science (No. GF201301003), and the Foundation of the State Key Laboratory of Solidification Processing in NWPU (No. SKLSP201306).

References

1. Dehghani K, Ghorbani R, Soltanipoor AR (2015) Microstructural evolution and mechanical properties during the friction stir welding of 7075-O aluminum alloy. Int J Adv Manuf Technol 77:1671–1679
2. Lotfi AH, Nourouzi S (2014) Predictions of the optimized friction stir welding process parameters for joining AA7075-T6 aluminum alloy using preheating system. Int J Adv Manuf Technol 73:1717–1737
3. Brandl E, Heckenberger U, Holzinger V, Buchbinder D (2012) Additive manufactured AlSi10Mg samples using selective laser melting (SLM): microstructure, high cycle fatigue, and fracture behaviour. Mater Des 34:159–169
4. Babajanzade Roshan S, Behboodi Jooibari M, Teimouri R, Asgharzadeh-Ahmadi G, Falahati-Naghibi M, Sohrabpoor H (2013) Optimization of friction stir welding process of AA7075 aluminum alloy to achieve desirable mechanical properties using ANFIS models and simulated annealing algorithm. Int J Adv Manuf Technol 69:1803–1818
5. ASTM F2792-10 Standard terminology for additive manufacturing technologies, July 2010
6. Baufeld B, van der Biest O, Gault R (2010) Additive manufacturing of Ti-6Al-4V components by shaped metal deposition: microstructure and mechanical properties. Mater Des 31:106–111
7. Terry W (2012) Wohlers report: additive manufacturing and 3D printing state of the industry, annual worldwide progress report. Wohlers Associate Inc 1–287
8. Wohlers TT (2010) Wohlers report 2010. Wohlers Associates, Fort Collins
9. Buchbinder D, Meiners W, Wissenbach K, Müller-Lohmeier K, Brandl E (2008) Rapid manufacturing of aluminium parts for serial production via selective laser melting (SLM). Aluminium Alloys. Aachen 2394–2400
10. Dehoff RR, Babu SS (2010) Characterization of interfacial microstructures in 3003 aluminum alloy blocks fabricated by ultrasonic additive manufacturing. Acta Mater 58(13):4305–4315
11. Mun J, Yun BG, Ju J, Chang BM (2015) Indirect additive manufacturing based casting of a periodic 3D cellular metal-flow simulation of molten aluminum alloy. J Manuf Process 17:28–40
12. Baufeld B, Van der Biest O, Gault R (2010) Additive manufacturing of Ti-6Al-4V components by shaped metal deposition: microstructure and mechanical properties. Mater Des 31:S106–S111
13. Louvis E, Fox P, Sutcliffe CJ (2011) Selective laser melting of aluminium components. J Mater Process Technol 211(2):275–284

14. Lodes MA, Guschlbauer R, Körner C (2015) Process development for the manufacturing of 99.94% pure copper via selective electron beam melting. Mater Lett 143:298–301
15. Sun SH, Koizumi Y, Kurosu S, Li YP, Chiba A (2015) Phase and grain size inhomogeneity and their influences on creep behavior of Co-Cr-Mo alloy additive manufactured by electron beam melting. Acta Mater 86:305–318
16. Buchbinder D, Schleifenbaum H, Heidrich S, Meiners W, Bültmann J (2011) High power selective laser melting (HP SLM) of aluminium parts. Phys Procedia 12:271–278
17. Dilip JJS, Babu S, Varadha Rajan S, Rafi KH, Janaki Ram GD, Stucker BE (2013) Use of friction surfacing for additive manufacturing. Mater Manuf Process 28:1–6
18. Dilip JJS, Janaki Ram GD, Stucker B (2012) Additive manufacturing with friction welding and friction deposition processes. Int J Rapid Manuf 3(1):56–69
19. Palanivel S, Nelaturu P, Glass B, Mishra RS (2015) Friction stir additive manufacturing for high structural performance through microstructural control in an Mg based WE43 alloy. Mater Des 65:934–952
20. Salari E, Jahazi M, Khodabandeh A, Ghasemi-Nanesa H (2014) Influence of tool geometry and rotational speed on mechanical properties and defect formation in friction stir lap welded 5456 aluminum alloy sheets. Mater Des 58:381–389
21. Zhang ZH, Yang XQ, Zhang JL, Zhou G, Xu XD, Zou BL (2011) Effect of welding parameters on microstructure and mechanical properties of friction stir spot welded 5052 aluminum alloy. Mater Des 32(8–9):4461–4470
22. Badarinarayan H, Yang Q, Zhu S (2009) Effect of tool geometry on static strength of friction stir spot-welded aluminum alloy. Int J Mach Tool Manuf 49(2):142–148
23. Yin YH, Sun N, North TH, Hu SS (2010) Hook formation and mechanical properties in AZ31 friction stir spot welds. J Mater Process Technol 210(14):2062–2070
24. Mao YQ, Ke LM, Liu FC, Liu Q, Huang CP, Xing L (2014) Effect of tool pin eccentricity on microstructure and mechanical properties in friction stir welded 7075 aluminum alloy thick plate. Mater Des 62:334–343
25. Prangnell PB, Heason CP (2005) Grain structure formation during friction stir welding observed by the 'stop action technique'. Acta Mater 53:3179–3192
26. İpekoğlu G, Erim S, Çam G (2014) Effects of temper condition and post weld heat treatment on the microstructure and mechanical properties of friction stir butt-welded AA7075 Al alloy plates. Int J Adv Manuf Technol 70:201–213
27. Sato YS, Urata M, Kokawa H, Ikeda K (2003) Hall-Petch relationship in friction stir welds of equal channel angular-pressed aluminium alloys. Mater Sci Eng A 354:298–305
28. Mahoney MW, Rhodes CG, Flintoff JG, Bingel WH, Spurling RA (1998) Properties of friction stir welded 7075 T651 aluminum. Metall Mater Trans A 29:1955–1964
29. Xu WF, Liu JH, Luan GH, Dong CL (2009) Temperature evolution, microstructure and mechanical properties of friction stir welded thick 2219-O aluminum alloy joints. Mater Des 30: 1886–1893